Indian Journal of Chemical Technology
Vol. 31, September 2024, pp. 710-721
DOI: 10.56042/ijct.v31i5.10300

Amendment of chitosan biopolymer with graphite for augmented confiscation of reactive blue-19 and reactive orange-16 textile dyes

P. M. Nandanwar[1]*, P. Doondani[1], D. Sarvanan[2] & R. M. Jugade[1]

[1]Department of Chemistry, RTM Nagpur University, Nagpur- 440 033, India

[2]Department of Chemistry, National College, Tiruchirappalli-620001, India

*E-mail: pradipnandanwar27@gmail.com

Received 9 April 2024; accepted 18 July 2024

In this work, we report the adsorption of reactive blue-19 (RB-19) and reactive orange-16 (RO-16) dyes from the aqueous solution onto chitosan-graphite composite (Chi-Gr). The adsorption of this textile dye has been tremendously improved after successfully immobilizing chitosan on graphite. The Chi–Gr has been characterized through Fourier transform infrared spectroscopy, X-ray diffraction, scanning electron microscopy, energy dispersive X-ray spectroscopy, and the pH point of zero charge for the physicochemical, structural and morphological analyses. The characterization of synthesized Chi-Gr indicates that the composite formation improves not only the surface chemistry but also its textural properties. Adsorption experiment reveals excellent adsorption capacity 123.21 mg of RB-19 dye and 62.16 mg per gram of Chi-Gr composite in accordance with Langmuir model with a coefficient of determination value of 0.9994 for RB-19 and 0.991 for RO-16 dyes. Furthermore, adsorption process follows pseudo-second order kinetics and thermodynamic equilibrium study revealed it's spontaneous, endothermic and entropy driven nature. The overall study demonstrates the importance of the synthesized adsorbent as potential candidature towards removal of RB-19 and RO-16 dyes from the wastewater.

Keywords: Adsorption, Chitosan, Graphite, Reactive blue-19, Reactive orange-16

Introduction

Enormous increase in the world population along with rapid modernization limits the availability of fresh water on earth due to variety of pollutants contaminate the water[1]. Among them, textile industry is the main contributor as it discharges the dyes to larger extent into the water bodies[2]. Growing dying industries produces high amount of wastewater containing various pollutants which significantly threaten the leaving and aquatic life as well due to discharge of untreated water into lakes and rivers[3]. Considering this, several techniques have been employed to capture the hazardous contaminants which pollute the environment. These techniques include chemical oxidation[4], coagulation[5], and filtration with coagulation[6], precipitation[7], and biological treatments[8]. However, the above mentioned methods have several limitations such as inherent sludge formation and its disposal in case of coagulation process[9]. In addition to that, operational cost also poses the concerns of its choices. Understanding the scenario, method of adsorption emerges out to be a premier process to remove dyes from effluents. Several activated carbon based materials[10], inorganic materials including metal oxides[11], carbon-based materials[12], organic materials includes especially metal–organic framework[13], and polymer-based materials[14] along with some bio-adsorbents[15] are hugely utilized for the removal of dye from effluents. The advantages of bio-adsorbents are easy to synthesize and its modification, inherently providing large surface area, variety of functional sites, high porosity, ease of reactivity, plenty of active sites, regeneration, reasonability and ultimately its high efficiency towards capture capacity for dangerous textile dye dissolved in waste water[16].

The ability of chitosan to remove contaminants from effluents is highly appreciated due to its diverse functionality, including amino and hydroxyl functional groups in the molecule for forming various interactions, including hydrogen bonding, electrostatic interaction, and van der Waals forces of attraction[17]. However, the insufficient strength and stability in acidic medium hinder the greater application of chitosan[18]. In order to resolve these issues and to improve the physicochemical properties of chitosan, its modifications using various crosslinkers as well as by composite formation with

mechanically and thermally stable materials are the most obvious pathways. Composites of chitosan with activated charcoal can be applied to improve the surface structure, morphology and surface-assimilative property of chitosan biopolymers[19]. Adding a crosslinking agent enhances the chemical stability and leads to microstructure improvement for its improved adsorption performance[20]. From ancient era, wastewater treatment traditionally been carried out using activated carbon due to the versatile nature, non-toxicity along with its diverse applications, however its usability follows some shortcomings such as it requires high cost of its regeneration and difficulties in its further modifications[21]. Meanwhile, graphene was found to be a more suitable candidate towards the carbon-based materials as an alternative. Being allotrope of carbon, graphene has wide surface area due to its layered structure[22]. Inherent aromaticity of graphene involves into π–π stacking with the contaminants[23] or use hydrophobic interactions[24] to remove efficiently the pollutants in the effluents. Again these materials have also been actively participating into the removal of various pollutants from the wastewater such as naptha-based contaminants[25] and various dyes[26].

The novelty of chitosan-graphite (Chi-Gr) composites in dye adsorption lies in their unique combination of properties that make them highly effective and efficient in removing dyes from wastewater. The incorporation of graphite into the chitosan matrix increases the surface area and porosity of the composite. This enhancement provides more active sites for dye adsorption, leading to higher adsorption capacities. The combination of chitosan and graphite results in a synergistic effect, where the composite exhibits superior adsorption properties compared to the individual components. This synergy arises from the improved dispersion of graphite in the chitosan matrix and the enhanced interaction between dye molecules and the composite. Chi-Gr composites can be tailored to selectively adsorb specific dyes based on their chemical structure. The functional groups in chitosan can be modified to target particular dye molecules, making the composite more effective for certain types of dyes. The high surface area and porosity of the Chi-Gr composite contribute to rapid adsorption kinetics. This means that the composite can quickly remove dyes from wastewater, making it suitable for real-time and large-scale applications. One of the significant advantages of Chi-Gr composites is their ability to be regenerated and reused multiple times without a significant loss in adsorption capacity. This feature enhances the sustainability and cost-effectiveness of the composite for dye removal applications. Both chitosan and graphite are environmentally friendly materials. The composite's use in dye adsorption aligns with sustainable practices, as it provides acost effective eco-friendly solution for wastewater treatment. Chi-Gr composites can be synthesized using relatively simple and scalable methods, such as solution mixing, in situ polymerization, and electrochemical deposition. These methods allow for the production of composites with controlled properties and high reproducibility. The composite can adsorb a wide range of dyes, including anionic, cationic, and non-ionic dyes. This versatility makes it a valuable material for treating various types of dye-contaminated wastewater[27.28].

In the recent years, our research group has reported bio-adsorbents including chitosan-sulphate cross-linked chitosan (SCC) and sulphate cross-linked chitosan–bentonite composite (SCC-B), Tetrabuty lammonium impregnated chitosan,chitosan-activated carbon composite (Cs–C) using sodium tripolyphosphate (STTP) as a crosslinker, chitosan-activated charcoal composite using sodium citrate as a crosslinker for the removal of toxic dyes[29-32]. In the current study, we are aiming to remove textile dye RB-19 and RO-16 from polluted water via the adsorption process using Chi-Gr adsorbent.

Experimental Section

Reagents

Chitosan with a degree of deacetylation >90% was purchased from Sisco Research Laboratory, India. Acetic acid and 25% NH_3 solution were obtained from SD Fine Chemicals Ltd (India). Graphite, Remazol brilliant blue R, Reactive Orange 16 dye were acquired from Loba Chemie (India). All the chemicals were of AR grade and used without further purification. Deionized distilled water was used throughout the studies.

Instrumentation

Fourier transform infrared (FTIR) spectra were recorded with a Bruker Alpha II spectrometer in the range 500–4000 cm^{-1} using KBr pellets. X-ray diffraction (XRD) were recorded on an Ultima IV diffractometer (Cu Kα radiation, 40 kV and 20 mA)

from 2θ = 2° to 10° with a step size of 0.02° (Rigaku, Tokyo, Japan).TESCAN VEGA 3 SBH was used for SEM micrographs andEnergy dispersive spectroscopy (EDAX) analysis was performed for elemental composition using an X-ray analyzer Oxford INCA Energy 250 EDS system during SEM observations. The thermal stability Chi-Gr was assessed in a DTG-60 simultaneous DTA/TG instrument (Shimadzu, Tokyo, Japan) in nitrogen medium. About 15 mg of the sample was loaded on a platinum pan with a heating rate of 20℃ min^{-1} up to 900℃ under 100 mL min^{-1} of flowing N_2. The samples were degassed at 150℃ for 2 h under vacuum and N_2 adsorption/desorption isotherms were acquired at −196℃ on a Quantachrome Nova 2200e analyzer (Anton Paar, Graz, Austria). The surface area was calculated by considering the BET model, and the pore volume was obtained using the BJH method. Equiptronics EQ-824 for spectrophotometer was used for recording absorption spectra of RB-19 and RO-16 dyes at respective wavelengths.

Synthesis of the adsorbent

Chitosan solution was prepared using a previously reported method by dissolving 5 g chitosan in 500 mL of 2% (weight) acetic acid under magnetic stirring for 60 min. After the complete dissolution of chitosan in acetic acid, 2 g graphite was added step by step and the solution was kept on gentle stirring for 5 h at 55℃. The resultant solution was dripped into a beaker containing 1000 mL of 6% (volume) ammonia solution with the help of a syringe, leading to the formation of spherical beads. The fresh beads were rinsed with distilled water several times for removal of all traces of ammonia. The resulting Chi–Gr beads were dried overnight in a hot air oven at 50℃. The beads were crushed by a pestle and mortar and sieved to 100 micron mesh before being used in the adsorption experiments.

Adsorption experiment

In each experiment, 25 mL dye (RB-19 and RO-16) solution of a predecided concentration along with a known weight of Chi-Gr, were stirred on a magnetic stirrer for a predetermined time. It was then filtered and the residual concentration of the solution was evaluated spectrophotometrically. Triplicate observations were obtained and the mean values were reported. The equilibrium adsorption efficiency (q_e) in mg g^{-1} was calculated as follows[33].

$$q_e = \frac{(C_0 - C_e)V}{W}$$

where C_o (mg L^{-1}) and C_e (mg L^{-1}) are the dye concentration initially and at equilibrium, respectively, while W (g) is the weight of adsorbent used in the respective study. Trial runs were performed to compare the adsorption efficiency of Chi-Gr adsorbent for the RB-19 and RO-16 dyes. For this, 50 mg L^{-1} dye solution was equilibrated for 60 min with 100 mg of Chi-Gr composite in different flasks. The solution phase concentrations in each flask were determined after filtration and the adsorption efficiency was calculated for each of them.

The pH_{PZC} of Chi-Gr was determined by a previously reported method[34] in order to establish the surface charge on the adsorbent. For this, 50 mL 0.1 M NaCl solutions with varying initial pH from 2.0 to 9.0 were taken in a series of conical flasks. These solutions were stirred with 100 mg of Chi-Gr for 24 h. The final pH of the supernatant solutions were measured.

A graph was plotted of the change in pH as a function of the initial pH, with the point it intersects the x-axis called the pH point of zero charge. For studying the effect of the initial solution pH on the adsorption efficiency, a series of dye solutions of 100 mg L^{-1} were prepared and their pH was varied from 4.0 to 9.0. To each of the systems, 100 mg of Chi-Gr adsorbent was administered and equilibrated for 30 min. After that, the systems were filtered and the absorbance values were obtained. The kinetics of adsorption was studied by equilibrating 100 mg L^{-1} dye solution with 25, 50 and 100 mg of Chi-Gr from 5 to 150 min. The residual solution phase dye concentration was determined after filtration.

In order to study the effect of the initial dye concentration, various dye concentrations from 20 to 400 mg L^{-1} were equilibrated with 25, 50 and 100 mg Chi-Gr for 60 min and then the dye concentration in the solution was determined.

The Chi-Gr dose was increased from 25 to 300 mg. Four dye concentrations of 50, 100, 150 & 200 mg L^{-1} were stirred with various doses of Chi-Gr for the optimized contact time of 60 min and then their final concentrations were determined spectro-photometrically. To study the effect of temperature as part of the evaluation of the thermodynamics parameters, the temperature was varied from 298 to 333 K. The quantity of adsorption of RB-19 and

RO-16 dyes upon Chi-Gr was investigated at an initial dye concentration of 100 mg L^{-1} using a 25 mL volume and adsorbent dose of 100 mg.

Results and Discussion

Material characterization

The composite was characterized using various techniques to understand the surface properties and interaction between the two constituents. The FT-IR spectrum of pure chitosan shows characteristic peaks at 1038 cm^{-1} (C-O-C stretching), 1523 cm^{-1} (N-H stretching), 2361 cm^{-1} (C-H stretching) and 654 cm^{-1} (C-H bending)[34]. When the composite Chi-Gr is formed, these bands shifted to 1049, 1529, 2454 and 673 cm^{-1} respectively. This shows electrostatic interaction between these groups and the carbon and oxidized carbon of graphite (Fig. 1a).

The SEM micrographs of chitosan and Chi-Gr have been presented in Fig. 1b and 1c, respectively, while the EDX spectrum of Chi-Gr has been shown in Fig. 1d. It can be seen that native chitosan has relative smooth surface leading to very low surface area (0.6 m^2 g^{-1}) while the surface of Chi-Gr was folded leading to enhancement in surface area (4.52 m^2 g^{-1}). The EDX spectrum showed peaks of carbon, nitrogen and oxygen.

The thermal stability studies were carried out using thermogravimetric analysis. The TGA and DTA curves of chitosan, graphite and Chi-Gr composite are shown in Fig. 2a, 2b, and 2c, respectively. It could be clearly seen that chitosan undergoes moisture loss around 100°C and single step degradation between 250-350°C. Pure graphite is thermally much stable that shows very slow weight loss. The composite shows properties of both chitosan as well as graphite. It shows typical weight loss between 250-350°C followed by slow weight loss similar to graphite. This is a clear indication of stability of Chi-Gr composite upto 300°C[35].

The XRD pattern of chitosan (Fig. 3) showed peaks due to (020) and (110) planes at 10.5 and 20.04°, respectively[36] while that of graphite showed sharp peak of (002) plane at 26.56° and a small but distinct peak of (004) plane at 56.64°. The Chi-Gr showed all of these peaks with slight shift in values indicating formation of composite[37].

The surface area of native chitosan was found to be 0.6 m^2g^{-1}. When chitosan forms a composite with graphite, the surface showed uneven morphology

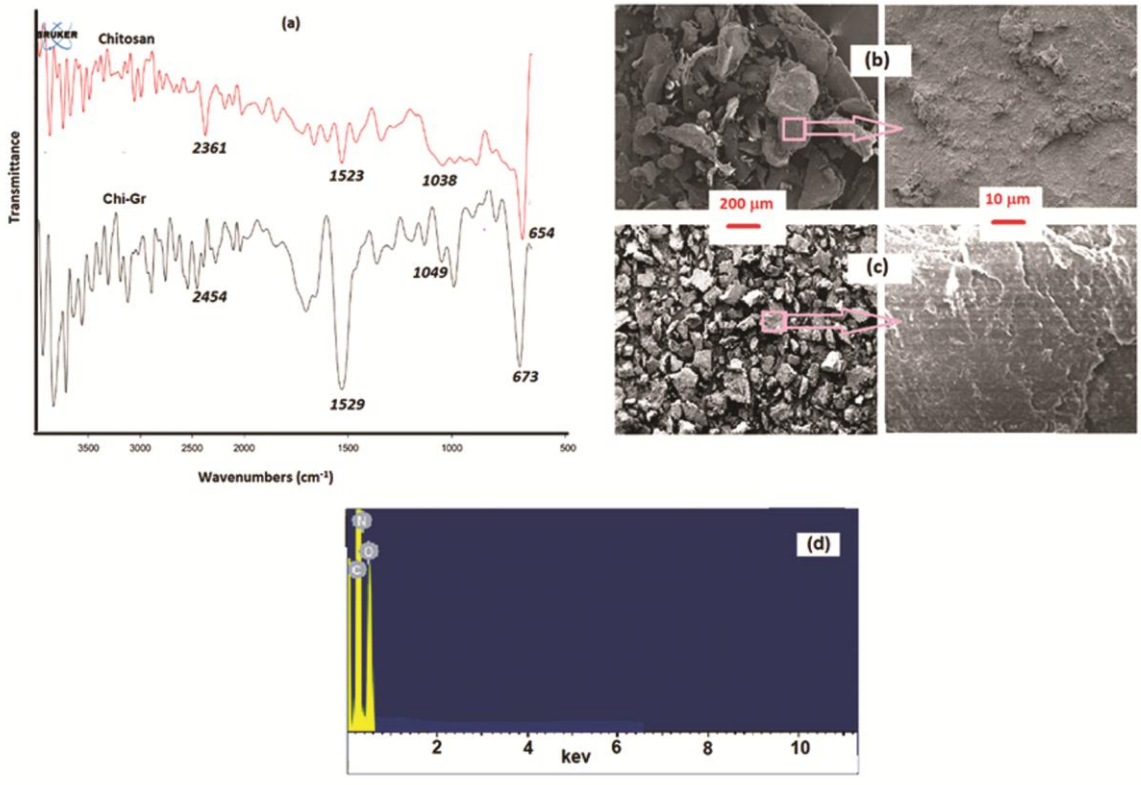

Fig. 1 — (a) FT-IR spectra, (b) SEM micrographs of chitosan and (c) SEM micrographs of Chi-Gr composite and (d) EDX spectrum of Chi-Gr composite

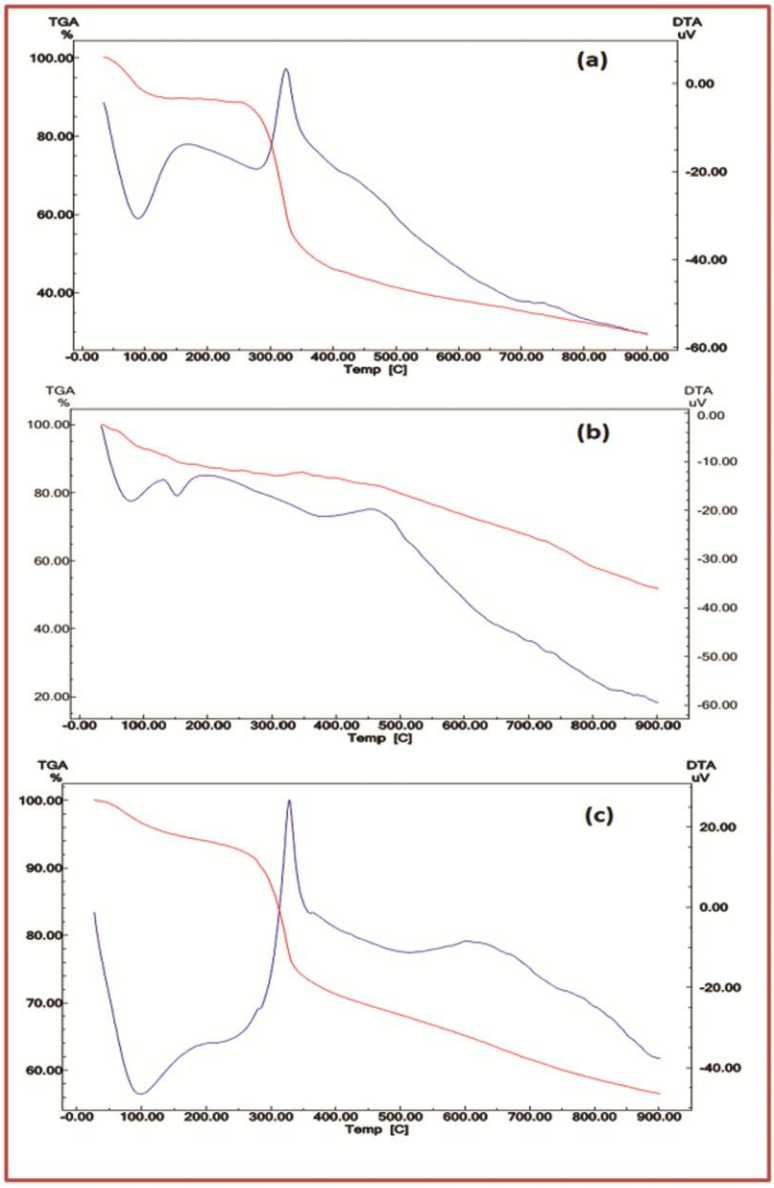

Fig. 2 — TGA (red) and DTA (blue) curves of (a) chitosan (b) graphite and (c) Chi-Gr

thereby increasing the surface area to 4.52 m^2g^{-1}. The nitrogen adsorption-desorption curve obtained from BET surface area analysis has been depicted in Fig. 4. The hysteresis between adsorption and desorption is an indication of H4 type isotherm as per IUPAC classification[38]. From the BJH analysis, it is clear that the material is mesoporous in nature with average pore radius of 30 nm.

Optimization of working parameters

The working parameters were optimized one by one keeping all other parameters constant. The pH of dye solution was changed from 3.0 to 9.0 taking 200 mg L^{-1} dye solution (25 mL) and stirred with 100 mg of Chi-Gr composite for 30 min. It was observed that pH does not cause any noteworthy effect over the entire range (Fig. 5a and 6a). Hence, further studies were carried out at the original solution pH of 6.0. This near-neutral pH gives an additional advantage of ability of the material to treat the effluents as received without maintaining pH. The pH_{pzc} of the composite was found to be 6.8 (Fig. 5b and 6b) indicating that the composite had positive charge at pH 6.0 and so, the anionic dye molecules undergo electrostatic attraction with it.

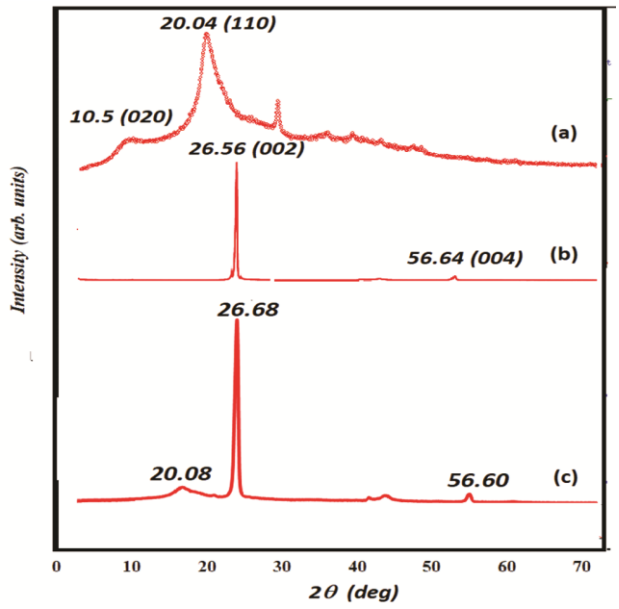

Fig. 3 — X-ray diffractograms of (a) chitosan (b) graphite and (c) Chi-Gr composite

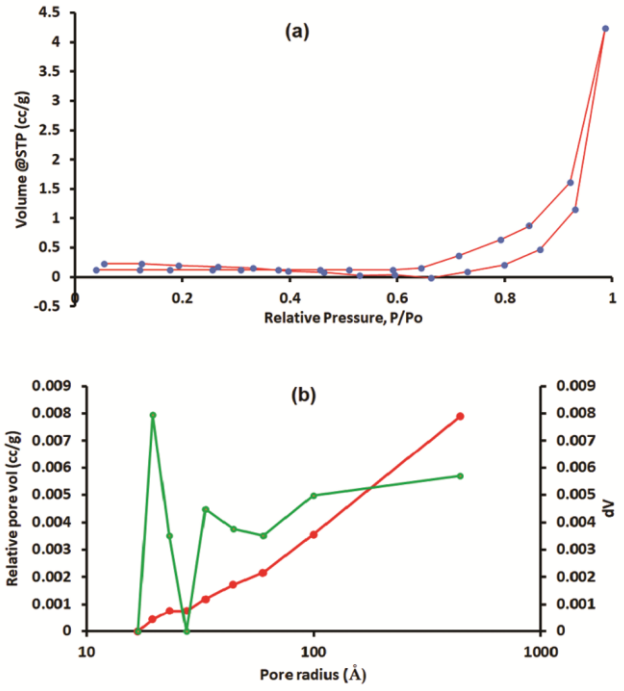

Fig. 4 — (a) Nitrogen adsorption-desorption curve and (b) pore size distribution of Chi-Gr

In order to study the effect of stirring time and to evaluate the kinetics parameters, the adsorption experiments were carried out for different time intervals (Fig. 5c and 6c). It was observed that the dye goes on adsorbing on the Chi-Gr surface rapidly initially. However, it leads to equilibrium in about 60 min and so this time was selected. With increase in amount of Chi-Gr, the percentage removal goes on increasing while the value of q (mg/g) increases upto 25 mg and decreases thereafter (Fig. 5d and 6d). This is due to availability of excess surface for adsorption above the optimum dose. In order to have effective adsorption, a dose of 50 mg was optimized, which is equivalent to a dose of just 2 g L^{-1}.

The solution concentration was varied to evaluate percentage removal as well as adsorption capacity *q*. It was observed that the removal percentage was decreasing with increasing dye solution concentration. However, with saturation of Chi-Gr surface, the adsorption efficiency went of decreasing but the adsorption capacity *q* went on increasing. This can be attributed to multilayer accumulation of RB-19 and RO-16, respectively, on Chi-Gr surface at higher dye concentration (Fig. 5e and 6e).

The solution temperature was increased from 303K to 333K to study the effect of temperature on adsorption efficiency and to evaluate the thermodynamic parameters. It was observed that the percentage removal goes on increasing with increase in temperature which is a typical behaviour of endothermic chemisorption phenomenon. The van't Hoff plot has been shown in Fig. 5f and 6f.

Isotherm, kinetics and thermodynamics studies

The data obtained from the adsorption experiments was subjected to analysis and evaluation for isotherm models, kinetic and thermodynamics parameters (Table 1 and 2). Graphical representation of various isotherm and kinetics models have been represented in Figs 7 and 8. It was observed that the adsorption followed Langmuir isotherm with coefficient of determination R^2 =0.998 and 0.991 for RB-19 and RO-16, respectively. It shows that the adsorption of RB-19 and RO-16 on Chi-Gr surface followed monolayer adsorption on homogeneous surface. The maximum adsorption capacity (q_m) as obtained from Langmuir isotherm was found to be 123.21 mg g^{-1} and 62.16 mg g^{-1}, for RB-19 and RO-16, respectively. Also, the value of Langmuir parameter RL was found to be 0.030 and 0.334 which is much less than 1 indicating favourable adsorption. This has been supported by the Freundlich parameter n = 2.704 and 0.753 which is between 1 and 10 showing favourable adsorption. The time-dependency data was subjected to pseudo-first-

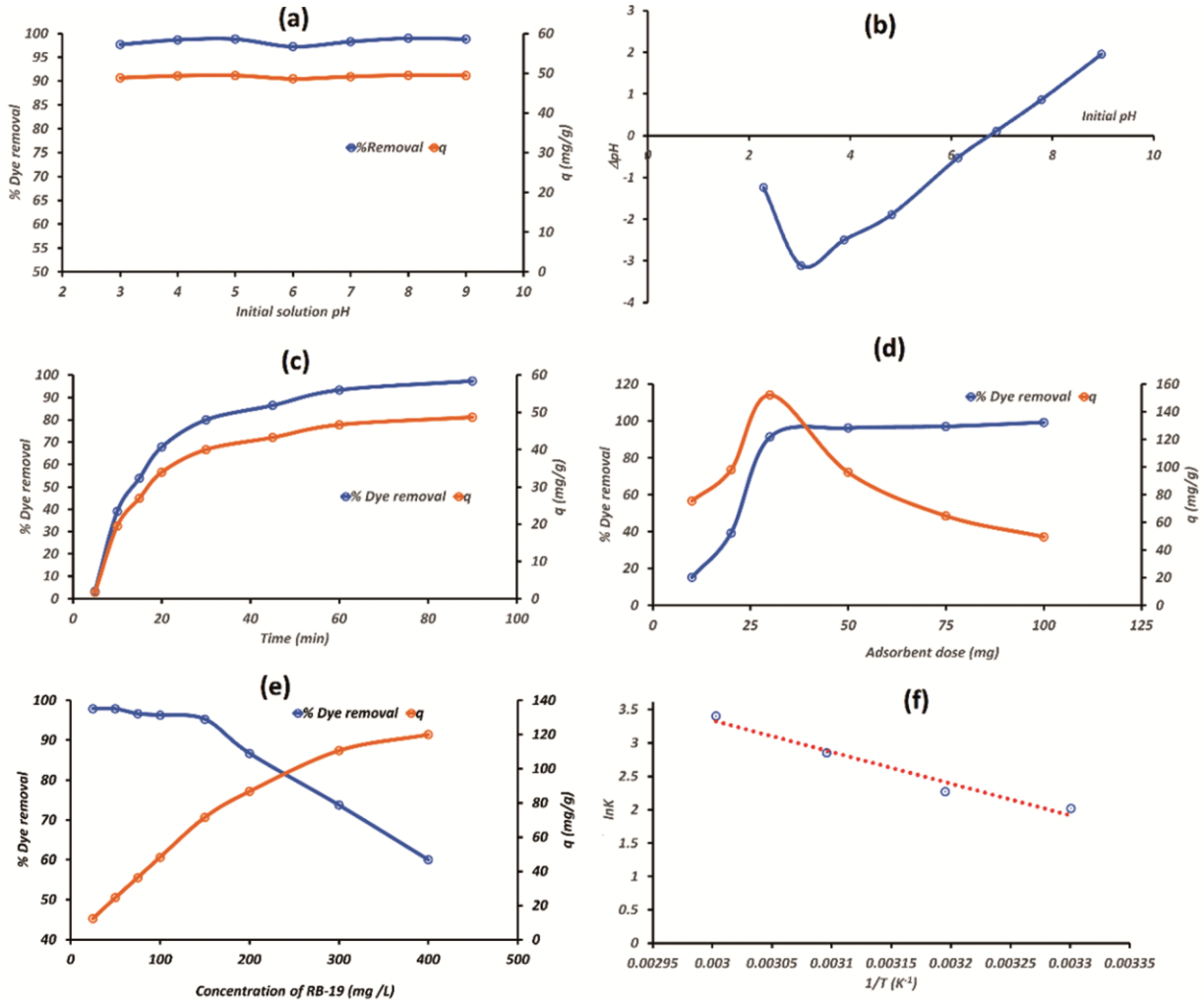

Fig. 5 — Effect of various working parameters (a) pH (b) pH_{pzc} (c) adsorption period (d) adsorbent dose (e) dye concentration and (f) temperature (van't Hoff plot) on adsorption of RB-19 dye

order (PFO) and pseudo-second-order (PSO) rate analysis. It was found to follow PSO kinetics with R^2 = 0.997 indicating chemisorption nature. The Weber- Morris IPD model shows that there is positive intercept for the graph between qt and $t_{1/2}$ indicating that the adsorption is not a diffusion control process (Fig. 7 and 8).

The evaluation of thermodynamics parameters was carried out using van't Hoff equation showing the value of free energy change becoming more negative with rise in temperature. For RB-19 adsorption, The free energy values (in kJ mol^{-1}) calculated for temperatures 298,313,318 and 323 K are -5.089, -5.902, -7.657 and -9.412, respectively. The enthalpy change ΔH and entropy change ΔS values at 298 K are 39.43 kJ mol^{-1} and 146.06 J mol^{-1} K^{-1}, respectively. The free energy values (in kJ mol^{-1}) calculated for temperatures 298,313,318 and 323 K are -4.306, -7.185, -8.365 and -9.488, respectively for RO-16 adsorption. The ΔH and ΔS values at 298 K are 57.028 kJ mol^{-1} and 205.63 J $mol^{-1}K^{-1}$, respectively. The positive value of enthalpy change suggests endothermic nature while positive value of entropy change suggests entropy driven nature of the adsorption.

Plausible mechanism

Graphite provided the surface for the chitosan molecules to interact with the dye ions with an anionic sulphate group. Chitosan has protonated amine groups that have a strong electrostatic interaction with the anionic dye molecules. This was in accordance with the observation that increasing the pH in the basic range reduced the adsorption capacity

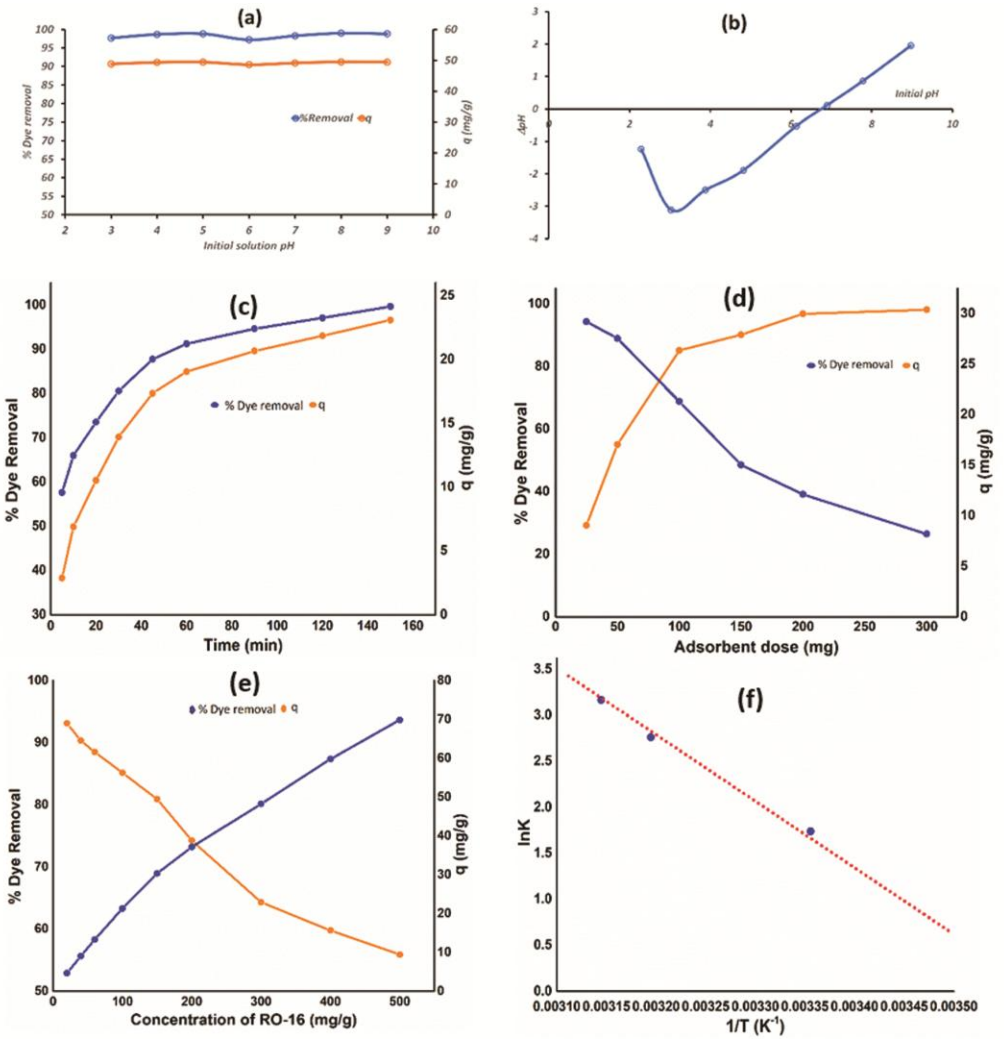

Fig. 6 — Effect of various working parameters (a) pH (b) pH_{pzc} (c) adsorption period (d) adsorbent dose (e) dye concentration and (f) temperature (van't Hoff plot) on adsorption of RB-16 dye

Table 1 — Isotherm, kinetics and thermodynamic values for RB-19 adsorption

Isotherms	Parameter	Values
Freundlich	K_f (mg L^{-1}/n $g^{-1}L^{-1}$)	23.76
	n	2.704
	R^2	0.896
Langmuir	q_m (mg g^{-1})	123.21
	b (L g^{-1})	0.158
	RL	0.030
	R^2	0.998
Rate model	Parameters	Values
Pseudo-first order	K_1 (min^{-1})	0.040
	R^2	0.976
Pseudo-second order	K_2 (L mol^{-1} min^{-1})	1.58 x 10^{-5}
	R^2	0.997
Intraparticle diffusion	K_{int}	11.56
	Intercept	4.01

Table 2 — Isotherm, kinetics and thermodynamic studies for RO-16 adsorption

Isotherms	Parameter	Values
Freundlich	K_f (mg L^{-1}/n $g^{-1}L^{-1}$)	1.944
	n	0.7529
	R^2	0.979
Langmuir	q_m(mg g^{-1})	62.16
	b (L g^{-1})	0.038
	RL	0.344
	R^2	0.991
Rate model	Parameters	Values
Pseudo-first order	K_1 (min^{-1})	0.0234
	R^2	0.985
Pseudo-second order	K_2 (L mol^{-1} min^{-1})	0.0035
	R^2	0.999
Intraparticle diffusion	K_{int}	1.571
	Intercept	7.83

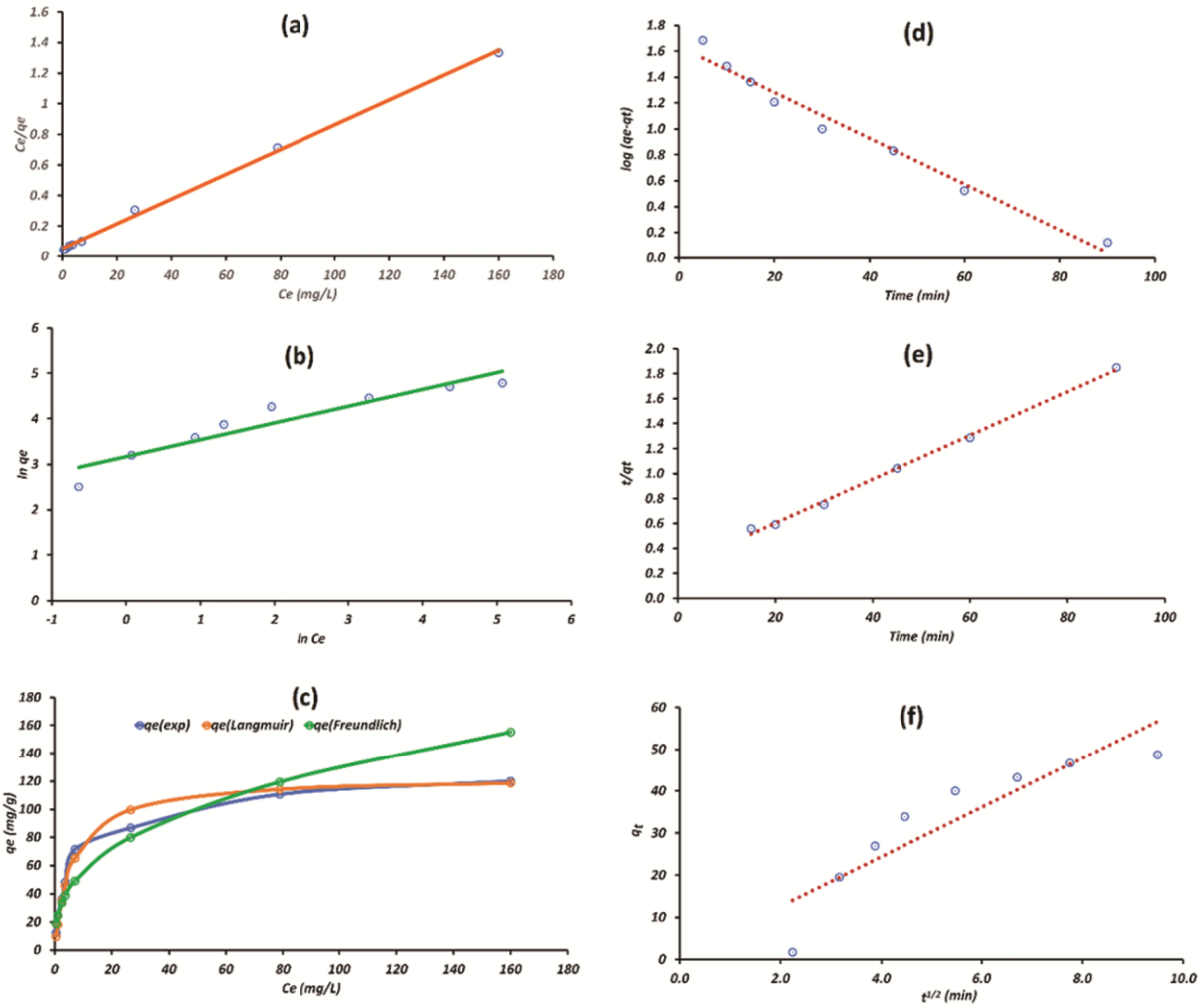

Fig. 7 — (a) Langmuir isotherm (b) Freundlich isotherm (c) C_e-q_e curve (d) PFO model (e) PSO model and (f) intraparticle diffusion model for RB-19 adsorption

Table 3 — Comparison of various adsorbents reported for Reactive dyes

Adsorbent	Anionic dyes	Capacity of absorption (mg/g)	References
Carbonized fish scale	R-16	105.8	38
Aqai palm stalk	R-16	62.9	39
Peanut hull	R-5	55.55	40
Fly Ash	RB-19	47.86	41
waste sludge	RB-19	91	42
activated carbon	RB-19	35.5	43
Fe–Al doped cellulose	RB-19	95.62	44
Polyurethane foam	R-21	8.31	45
Fomes fomentarius	RB-19	90	46
Sewage sludge	R-16	114.7	47
Biomass	RB-19	103	48
Chi-Gr	RB-19	123.21	Present work
Chi-Gr	R-16	62.16	Present work

of Chi-Gr and also as the $-NH_2$ peak was suppressed after adsorption of the dye molecules. At pH 6.0, the composite surface is positively charged as indicated by the pH_{pzc} studies. At this pH, the negative sulphate group of anionic dye RB-19 and RO-16 interacts with ammonium group of chitosan leading to strong electrostatic interaction as shown in Fig. 9.

Comparison with literature

The synthesized composite Chi-Gr has been compared with various materials already reported in literature on the basis of their adsorption capacities. The comparison has been shown in Table 3 which is self-explanatory. It shows that the q_{max} value of Chi-Gr is much higher than most of the reported adsorbents.

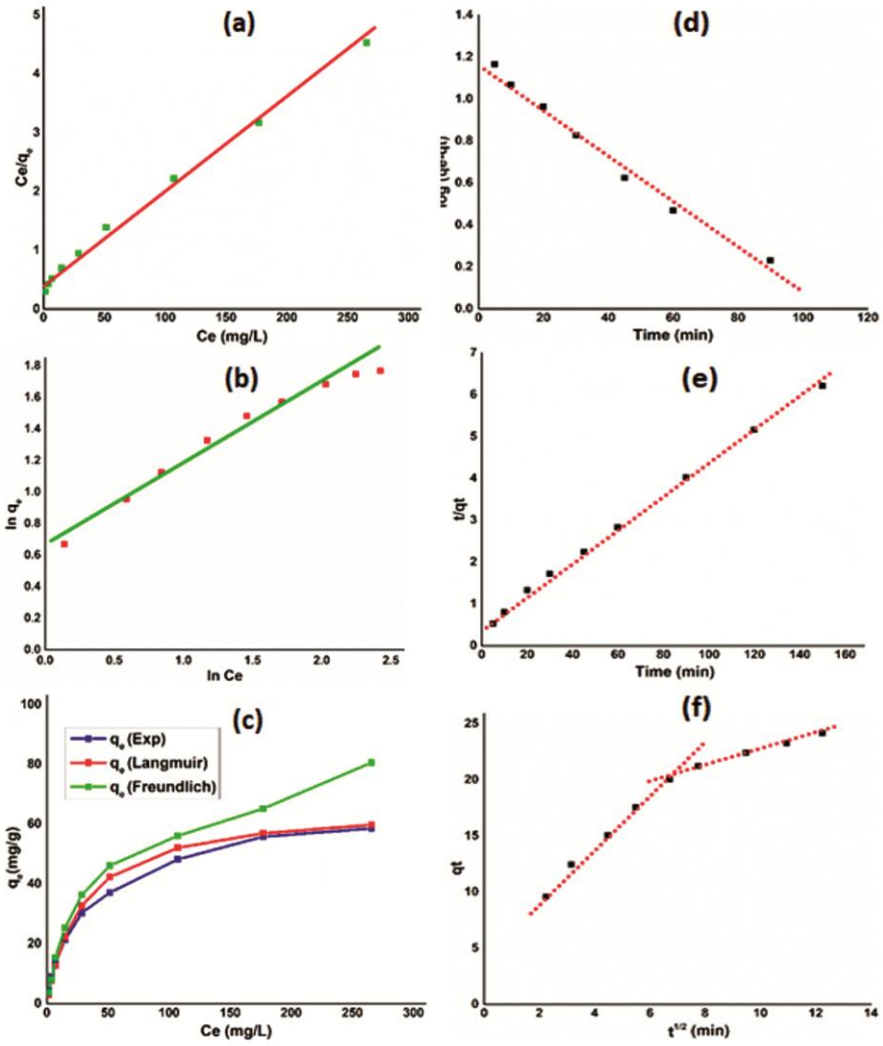

Fig. 8 — (a) Langmuir isotherm (b) Freundlich isotherm (c) C_e-q_e curve (d) PFO model (e) PSO model and (f) intraparticle diffusion model for RB-16 adsorption

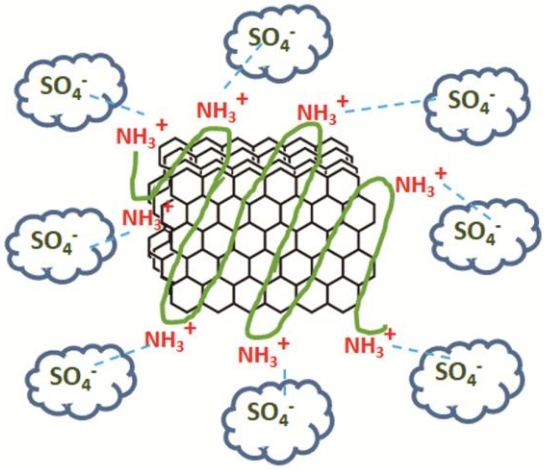

Fig. 9 — Plausible mechanism of Chitosan-Graphite Composite Interaction with RB-19 and RO-16

Conclusion

Chitosan was used to entrap graphite leading to enhancement of its overall surface area. The characterization of Chi-Gr showed modifications in surface morphology as well as elemental composition confirming composite formation. The novelty of chitosan-graphite composites in dye adsorption is derived from their high adsorption capacity, enhanced surface area and porosity, synergistic effects, selective adsorption capabilities, rapid kinetics, regeneration and reusability, environmental friendliness, ease of synthesis, versatility and cost-effectiveness. These properties make them a promising and innovative solution for the effective removal of dyes from wastewater. The adsorption for RB-19 and RO-16 was found to be substantial with capacity of

123.21 mg g^{-1} and 62.16 mg g^{-1}, respectively in accordance with Langmuir model. Spontaneous, endothermic and entropy driven nature of the dye confiscation process were proved by the van't Hoff plot analysis. The adsorption of RB-19 dye could be attributed to various interactions like electrostatic force, hydrogen bonding as well as π-π electronic interactions. In short, the material has a number of merits over those reported in literature that include ease of synthesis, short span of adsorption time, near-neutral pH of adsorption and high efficiency to adsorb anionic dyes. In future, the Chi-Gr composite can be utilized in various fields such as biomedical, environmental, energy storage and conversion, sensors, electronics, food packaging, agriculture and coatings and films.

Acknowledgement

The authors are grateful to RTM Nagpur University for instrumentation and laboratory facilities. Thanks are due to DST, New Delhi for DST-FIST grant and UGC for UGC-SAP support.

References

1 Lu F & Astruc D, Nanocatalysts and other nanomaterials for water remediation from organic pollutants, *Coord Chem Rev*, 408 (2020) 213180.
2 Wong J, Tan H, Lau S, Yap P & Danquah M, Potential and challenges of enzyme incorporated nanotechnology in dye wastewater treatment: A review, *J Environ Chem Eng*, 7 (2019) 103261.
3 Nithya R, Thirunavukkarasu A, Sathya A & Sivashankar R, Magnetic materials and magnetic separation of dyes from aqueous solutions: A review, *Environ Chem Lett*, 19 (2021) 1275.
4 Senapati S, Srivastava S, Singh S & Kulkarni A, SERS active Ag encapsulated Fe@ SiO_2 nanorods in electromagnetic wave absorption and crystal violet detection, *Environ Res*, 135 (2014) 95.
5 Mcyotto F, Wei Q, Macharia D, Huang M, Shen C & Chow C, Effect of dye structure on color removal efficiency by coagulation, *Chem Eng J*, 405 (2021) 126674.
6 Piaskowski K, Świderska-Dąbrowska R & Zarzycki P, Dye removal from water and wastewater using various physical, chemical and biological processes, *J AOAC Int*, 101 (2018) 1371.
7 Anushree C & Philip J, Efficient removal of methylene blue dye using cellulose capped Fe_3O_4 nanofluids prepared using oxidation-precipitation method, *Colloids Surf A*, 567 (2019) 193.
8 Paz A, Carballo J, Pérez M & Domínguez J, Biological treatment of model dyes and textile wastewaters, *Chemosphere*, 181 (2017) 168.
9 Semblante G, Lee J, Lee L, Ong S & Ng H, Brine pre-treatment technologies for zero liquid discharge systems, *Desalination*, 441 (2018) 96.
10 Moosavi S, Lai C, Akbarzadeh O & Johan M, Recycled activated carbon-based materials for the removal of organic pollutants from wastewater, *Waste Recycl Technol Nanomater Manuf*, (2021) 513.
11 Maity C, Sahoo S, Verma K, Behera A & Nayak G, Facile functionalization of boron nitride (BN) for the development of high-performance asymmetric supercapacitors, *New J Chem*, 44 (2020) 8106.
12 Zhou Y, Lu J, Zhou Y & Liu Y, Recent advances for dyes removal using novel adsorbents: A review, *Environ Pollut*, 252 (2019) 352.
13 Chafai H, Laabd M, Elbariji S, Bazzaoui M & Albourine A, Study of congo red adsorption on the polyaniline and polypyrrole, *J Disper Sci Technol*, 38 (2017) 832.
14 Mohanty C, Mishra P, Samal A, Das N & Behera A, Design of inexpensive, magnetically separable $MnFe_2O_4$/poly meta-amino phenol (PmAP) heterostructure: Catalyst for bisphenol A & reactive blue 19 mineralisation, *Environ Sci Adv*, 3 (2024) 561.
15 Hasan M, Shenashen M, Hasan M, Znad H, Salman M & Awual M, Natural biodegradable polymeric bioadsorbents for efficient cationic dye encapsulation from wastewater, *J Mol Liq*, 323 (2021) 114587.
16 Basnet P & Zhao Y, Superior dye adsorption capacity of amorphous WO_3 sub-micrometer rods fabricated by glancing angle deposition, *J Mater Chem A*, 2 (2014) 911.
17 Zhou Y, Lu J, Zhou Y & Liu Y, Recent advances for dyes removal using novel adsorbents: A review, *Environ Pollut*, 252 (2019) 352.
18 Elsabee M, Morsi R & Al-Sabagh A, Surface active properties of chitosan and its derivatives, *Colloids Surf B*, 74 (2009) 1.
19 Guo M, Wang J, Wang C, Strong P, Jiang P, Ok Y & Wang H, Carbon nanotube-grafted chitosan and its adsorption capacity for phenol in aqueous solution, *Sci Total Environ*, 682 (2019) 340.
20 Yang J, Han Y, Sun Z, Zhao X, Chen F, Wu T & Jiang Y, PEG/sodium tripolyphosphate-modified chitosan/activated carbon membrane for Rhodamine B removal, *ACS Omega*, 6 (2021) 15885.
21 Altmann J, Ruhl A, Zietzschmann F & Jekel M, Direct comparison of ozonation and adsorption onto powdered activated carbon for micropollutant removal in advanced wastewater treatment, *Water Res*, 55 (2014) 185.
22 Mohanty C, Das N, Behera A & Tripathy B, Efficiency of poly (m-aminophenol) as a novel adsorbent for individual/simultaneous removal of organic dyes and hexavalent chromium from water sources, *Water Air Soil Pollut*, 234 (2023) 204.
23 Kemp K, Seema H, Saleh M, Le N, Mahesh K, Chandra V & Kim K, Environmental applications using graphene composites: Water remediation and gas adsorption, *Nanoscale*, 5 (2013) 3149.
24 Mishra P, Das P, Paul S, Das P, Manna S, Basak P & Behera A, Graphene oxide dots-loaded chitin flask: A sustainable adsorbent for separating multiple dyes from water, *Environ Qual Manag*, 34 (2024).
25 Maswanganyi S, Gusain R, Kumar N, Fosso-Kankeu E, Waanders F & Ray S, Bismuth molybdate nanoplates supported on reduced graphene oxide: An effective nanocomposite for the removal of naphthalene via adsorption-photodegradation, *ACS Omega*, 6 (2021) 16783.

26 Yang B, Tian Z, Zhang L, Guo Y & Yan S, Enhanced heterogeneous fenton degradation of methylene blue by nanoscale zero valent iron (nZVI) assembled on magnetic Fe_3O_4/reduced graphene oxide, *J Water Process Eng*, 5 (2015) 101.

27 Qin Y, Yang H & Dong S, Eco-friendly chitosan-graphite composite for efficient dye removal from wastewater, *Environ Technol Innov*, 15 (2019) 100406.

28 Li Y, Zhu K & Wang S, Polycentric and dispersed population distribution increases PM 2. 5 concentrations: Evidence from 286 Chinese cities, 2001–2016, *J Clean Prod*, 248 (2020) 119202.

29 Khapre M & Jugade R, Hierarchical approach towards adsorptive removal of Alizarin red S dye using native chitosan and its successively modified versions, *Water Sci Technol*, 82 (2020) 715.

30 Khapre, M & Jugade, R, Tetrabutylammonium impregnated chitosan for adsorptive removal of harmful carcinogenic dyes from water-bodies, *Chemistry Africa*, 4 (2021) 993-1005.

31 Nandanwar P, Saravanan D, Bakshe P & Jugade R, Chitosan entrapped microporous activated carbon composite as a supersorbent for remazol brilliant blue R, *Mater Adv*, 3 (2022) 5488.

32 Nandanwar P, Jugade R, Gomase V, Shekhawat A, Bambal A, Saravanan D & Pandey S, Chitosan-biopolymer-entrapped activated charcoal for adsorption of reactive orange dye from aqueous phase and CO_2 from gaseous phase, *J Compos Sci*, 7 (2023) 103.

33 Kenawy E, Ghfar A, Wabaidur S, Khan M, Siddiqui M, Alothman Z & Hamid M, Cetyltrimethylammonium bromide intercalated and branched polyhydroxystyrene functionalized montmorillonite clay to sequester cationic dyes, *J Environ Manag*, 219 (2018) 285.

34 Kahu S, Shekhawat A, Saravanan D & Jugade R, Ionic solid-impregnated sulphate-crosslinked chitosan for effective adsorption of hexavalent chromium from effluents, *Int J Environ Sci Technol*, 13 (2016) 2269.

35 Korde S, Tandekar S & Jugade R, Novel mesoporous chitosan-zirconia-ferrosoferric oxide as magnetic composite for defluoridation of water, *J Environ Chem Eng*, 8 (2020) 104360.

36 Vithalkar S & Jugade R, Adsorptive removal of crystal violet from aqueous solution by cross-linked chitosan coated bentonite, *Mater Today: Proc*, 29 (2020) 1025.

37 Ain Q, Haq S, Alshammari A, Al-Mutlaq M & Anjum M, The systemic effect of PEG-nGO-induced oxidative stress in vivo in a rodent model, *Beilstein J Nanotechnol*, 10 (2019) 901.

38 Marrakchi F, Ahmed M, Khanday W, Asif M & Hameed B, Mesoporous carbonaceous material from fish scales as low-cost adsorbent for reactive orange 16 adsorption, *J Taiwan Inst Chem Eng*, 71 (2017) 47.

39 Cardoso N, Lima E, Calvete T, Pinto I, Amavisca C, Fernandes T & Alencar W, Application of aqai stalks as biosorbents for the removal of the dyes reactive black 5 and reactive orange 16 from aqueous solution, *J Chem Eng Data*, 56 (2011) 1857.

40 Tanyildizi M S, Modeling of adsorption isotherms and kinetics of reactive dye from aqueous solution by peanut hull, *Chem Eng J*, 168 (2011) 1234.

41 Dizge N, Aydiner C, Demirbas E, Kobya M & Kara S, Adsorption of reactive dyes from aqueous solutions by fly ash: Kinetic and equilibrium studies, *J Hazard Mater*, 150 (2008) 737.

42 Santos S, Vilar V & Boaventura R, Waste metal hydroxide sludge as adsorbent for a reactive dye, *J Hazard Mater*, 153 (2008) 999.

43 Silva T, Ronix A, Pezoti O, Souza L, Leandro P, Bedin K & Almeida, V, Mesoporous activated carbon from industrial laundry sewage sludge: Adsorption studies of reactive dye remazol brilliant blue R, *Chem Eng J*, 303 (2016) 467.

44 Khapre M, Shekhawat A, Saravanan D, Pandey S & Jugade R, Mesoporous Fe–Al-doped cellulose for the efficient removal of reactive dyes, *Mater Adv*, 3 (2022) 3278.

45 da Silveira N J, Moreira G, da Silva C, Reis C & Reis E, Use of polyurethane foams for the removal of the direct red 80 and reactive blue 21 dyes in aqueous medium, *Desalination*, 281 (2011) 55.

46 Arslantaş C, M'barek I, Saleh M, Isik Z, Ozdemir S, Dundar A & Dizge N, Basic red 18 and remazol brilliant blue R biosorption using russula brevipes, agaricus augustus, fomes fomentarius, *Water Pract Technol*, 17 (2022) 749.

47 Won S, Choi S & Yun Y, Performance and mechanism in binding of reactive orange 16 to various types of sludge, *Biochem Eng J*, 28 (2006) 208.

48 Aracagök Y, Biosorption of remazol brilliant blue R dye onto chemically modified and unmodified yarrowia lipolytica biomass, *Arch Microbiol*, 204 (2022) 128.